



Seasonal mass balance drivers for Swiss glaciers over 2010-2024 inferred from remote-sensing observations and modelling

Cremona Aaron^{1,2}, Matthias Huss^{1,2,3}, Johannes Landmann⁴, Mauro Marty⁵, Marijn van der Meer^{1,2}, Christian Ginzler⁵, and Daniel Farinotti^{1,2}

¹Laboratory of Hydraulics, Hydrology and Glaciology (VAW), ETH Zurich, Zurich, Switzerland

²Swiss Federal Institute for Forest, Snow and Landscape Research (WSL), bâtiment ALPOLE, Sion, Switzerland

³Department of Geosciences, University of Fribourg, Fribourg, Switzerland

⁴Federal Office of Meteorology and Climatology MeteoSwiss, Zurich-Airport, Switzerland

⁵Swiss Federal Institute for Forest, Snow, and Landscape Research (WSL), Birmensdorf, Switzerland

Correspondence: Aaron Cremona (cremona@vaw.baug.ethz.ch)

Abstract. Reliable estimates of glacier mass balance for an entire mountain range provide valuable insights into the impact of glacier melt on regional water resources. Here, we derive daily mass balance estimates for every glacier in the Swiss Alps over the period 2010-2024. To do so, we leverage a glaciological model and remote sensing observations, i.e. geodetic volume changes and observations of the snow-covered area fraction (SCAF) of glaciers during summer, together with machine-learning techniques for extrapolation purposes. This allows reproducing the seasonal variability of glacier mass balance for glaciers without in situ observations and determining daily glacier mass balance across Switzerland. Over the study period, the Swiss glaciers lost almost 25% of their 2010 ice volume, which corresponds to a wastage of $-15.2 \pm 1.6 \text{ km}^3$ of ice. The highest winter snow accumulation is inferred to occur in central and western Switzerland, with up to 1.5-1.9 m w.e. by the end of April, whereas the lowest winter accumulation is detected in Valais and ranges between 0.9-1.2 m w.e. Furthermore, winter balances are found to show better correlation in space compared to long-term annual balances, which range between -0.6 and -1.5 m w.e., indicating different dominating mechanisms. Finally, we assessed the spatio-temporal variability of seasonal mass balance to gain in-depth insights into the relation between glacier mass balance and the driving climatic factors in the Swiss Alps.

1 Introduction

Glaciers are rapidly retreating due to global warming (Hugonnet et al., 2021; The GLAMBIE Team, 2025), and monitoring the evolution of these components of the cryosphere is important to understand the driving processes involved, to assess their impact on natural hazards (Stoffel and Huggel, 2012) and water resources (Immerzeel et al., 2020), and to address the growing public interest in their changes. In the Swiss Alps, glaciers play a key role in the hydrological cycle, storing water over the winter and supplying it in the summer (van Tiel et al., 2025). Therefore, the availability of fresh water in Switzerland is strongly



20 impacted by glaciers (Pellicciotti et al., 2014; Radić and Hock, 2014; Schaeffli et al., 2019), but the water supplied by glaciers in the future is expected to decrease due to climate change and shrinking glaciers (Salzmann et al., 2012; Farinotti et al., 2016; Huss and Hock, 2018; Dumont et al., 2025). This leads to increasing interest in accurate monitoring of glacier mass balance and runoff on the regional scale (Anghileri et al., 2018; Patro et al., 2018; Dussaillant et al., 2025).

A widely used technique for evaluating regional mass balances is the geodetic method, which relies on differencing Digital
25 Elevation Models (DEMs) to derive changes in the elevation of the glacier surface and thus derive changes in ice volume (Dussaillant et al., 2018; Denzinger et al., 2021; Hugonnet et al., 2021; Piermattei et al., 2024; The GLAMBIE Team, 2025). The use of this technique over short periods is linked to several challenges due to snow and firn densification processes (Huss, 2013), although recent studies proved the application potential over short periods relying on very high-resolution images (Klug et al., 2018; Vincent et al., 2021; Zeller et al., 2022; Beraud et al., 2023). Geodetic mass balance calculations are, however, still
30 mostly performed over longer time spans, i.e., usually more than five years, allowing for the limitation of uncertainties.

A well-suited approach for bridging this temporal gap and, thus, deriving glacier mass balance over shorter time scales is to combine geodetic mass balance estimates with modelling approaches (Huss et al., 2008; Compagno et al., 2021; Rounce et al., 2023). This was done extensively in the past to reconstruct glacier mass balance time series or to model the future evolution of glaciers based on calibrated models (Hock et al., 2019; Zekollari et al., 2019; Rounce et al., 2020). Despite the
35 proven reliability of these examples for estimating annual balances, capturing the seasonal variations of mass balance remains a significant challenge (Barandun et al., 2021; Schuster et al., 2023; Cremona et al., 2025). This is a consequence of the limited observations available to constrain models, which leads to parameter equifinality and thus to inaccurately constrained seasonal variability (Finger et al., 2011; Gabbi et al., 2014). For that reason, current estimates of the seasonal glacier mass balance at the scale of the Swiss Alps are calculated based on statistical upscaling of the seasonal variability inferred from a set of about
40 20 glaciers with seasonal in situ observations (GLAMOS, 2024c; van Tiel et al., 2025). However, a comprehensive quantitative analysis with high spatio-temporal resolution at the regional scale relying on glacier-specific modelling and remote sensing observations is still lacking.

Several studies suggested different strategies to incorporate remote-sensing observations at high temporal resolution, which are often available at the scale of entire regions, to better constrain glacier mass balance (Hock et al., 2007; Huss et al., 2013; Hulth et al., 2013; Barandun et al., 2018, 2021). One of the most recent approaches, presented by Cremona et al. (2025),
45 constrains the seasonal variability of glacier mass balance by relying on observed mean mass balances and observation of the snow-covered area fraction (SCAF), derived from weekly to monthly satellite imagery, together with a glaciological model. In this study, we employ this approach to derive daily mass balance estimates for each of the 1400 glaciers in the Swiss Alps over the period 2010-2024. In contrast to Cremona et al. (2025), here we additionally account for the effect of supraglacial debris
50 cover and changing glacier area, which is relevant for regional-scale assessments (Elsberg et al., 2001; Rounce et al., 2021). Some Swiss glaciers are strongly debris-covered and small glaciers experienced significant changes in area over the 15-year study period (Linsbauer et al., 2021). Therefore, these effects cannot be neglected.

Regional mass balance estimates are strongly dependent on the geodetic mass balance (Zemp et al., 2019; The GLAMBIE Team, 2025). The last complete assessment of geodetic mass balance covering all glaciers of the Swiss Alps spans the period



1980-2010 (Fischer et al., 2015). Therefore, considering the extreme changes the Swiss glaciers experienced in the last decade (Cremona et al., 2023; GLAMOS, 2024a), we calculate changes in ice volume by differentiating a large set of DEMs from different sources for the Swiss glaciers between 2006-2023. These ice volume changes are then combined with SCAF observations derived from Sentinel-2 (available from 2015 to 2021) to constrain model parameters during calibration. This procedure is applied to 87 mostly large glaciers with available SCAF observations, which are distributed across all regions of Switzerland. Then, the model parameters are extrapolated using machine learning to the rest of the glaciers, and the daily mass balance for every glacier in the Swiss Alps over 2010-2024 is extracted. We derive changes in ice volume for the Swiss Alps over the study period. We assess regional differences in mass balance and its daily to annual temporal variability, identifying and discussing the main climatic drivers for glacier mass balance in Switzerland. Finally, we compare our results with existing estimates from upscaling approaches, i.e. (GLAMOS, 2024c), and discuss the strengths and limitations of the individual methodologies.

2 Study Site and Data

According to the last Swiss Glacier Inventory (SGI Linsbauer et al., 2021), the Swiss Alps comprised 1400 glaciers, resulting in a total glacierized area of 961 km² by the year 2016 (Fig. 1). For 1344 glaciers (98% of the total glacier area) a set of multiple DEMs is available over the study period, allowing us to derive geodetic ice volume changes (see Sect. 3.1, Fig. 1). The DEMs used in this study are derived from aerial images acquired by the Swiss Federal Office of Topography (swisstopo) over the period 2006-2023. Swisstopo acquires a first set of aerial images within the standard program covering all of Switzerland following a 3-year cycle (swisstopo, 2022). Furthermore, a second set of images is acquired annually by swisstopo within the so-called "cryospheric monitoring flights" (swisstopo, 2024), aiming at detailed monitoring of selected glaciers in the frame of the Glacier Monitoring Switzerland (GLAMOS) programme. The high-resolution (0.10-0.25 m) aerial images from both image sets are then processed following two separate pipelines to derive DEMs on glaciers. The first pipeline was developed by the Swiss National Forest Inventory (SNFI) and processes images from the standard 3-year-cycle program to deliver DEMs that were primarily designed for lowland applications (Ginzler and Hobi, 2015), thus partially resulting in lower quality over high-mountain regions and glaciers. Due to this, two additional processing steps are necessary for these DEMs. In the first step, each DEM is decomposed into the original DEM stripes resulting from different flight lines. These DEM stripes are then realigned, enhancing the relative orientation between adjacent flight lines. This happens with the OPALS Least Square Matching algorithm in overlapping areas (Pfeifer et al., 2014). In the second step, the resulting, now corrected DEM, is aligned to a common, Swiss-wide stable terrain DEM. The latter is chosen to be the swissAlti3D DEM of 2018. This two-step procedure allows for increasing the internal consistency of the SNFI DEMs over glaciers, thus enabling ice volume change calculations. The second pipeline follows the standard processing chain of swisstopo and is based on an automated procedure relying on stereo correlation and photogrammetric methods, which sometimes includes information from stereoscopic 3D measurements and available laser measurements manually. More detailed information is provided by swisstopo (2022). This pipeline processes aerial images from both image sets mentioned above. All available DEMs (with a resolution of 0.5-2.0 m), resulting from both pipelines, are used to derive multiple estimates of the ice volume change over the study period (see Sect. 3.1).

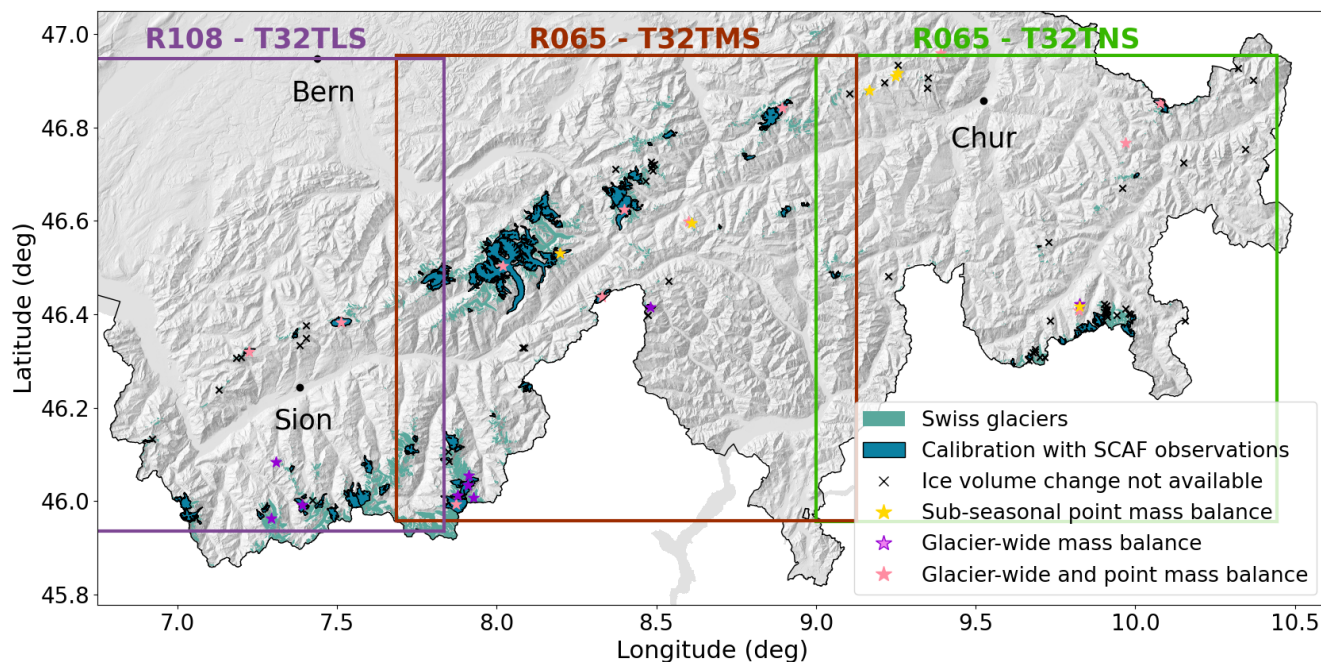


Figure 1. Overview of the study region. Glaciers are shown in teal. The 87 glaciers for which we apply the calibration with SCAF observations (see Sect. 3.2.3) are highlighted in dark teal. For the remaining glaciers, the model parameters are extrapolated relying on a machine learning approach (Sect. 3.2.4). Ice volume changes are available for 1344 glaciers. Glaciers without ice-volume change information (black crosses) and glaciers used for validation (coloured stars) are shown separately. For the latter, glaciers with sub-seasonal point mass balance observations (yellow stars), glaciers with seasonal glacier-wide mass balance observations (violet stars), and glaciers with both types of observations (pink stars) are distinguished. The footprints of the Sentinel-2 tiles R108-T32TLS, R065-T32TMS, and R065-T32TNS for extracting SCAF are shown in purple, red, and green, respectively.

For 87 glaciers (highlighted in dark blue in Fig. 1), we apply a calibration relying on SCAF observations over the melt season and geodetic ice volume changes (see Sect. 3.2.3). For the remaining ~ 1300 glaciers, the model parameters are extrapolated relying on a machine-learning approach and information on geodetic ice volume changes (see Sect. 3.2.4). The SCAF observations were derived by Schwaizer et al. (2023); Cremona et al. (2025) from Sentinel-2 multi-spectral L1C data during the melt seasons (June - September) over 2015-2021, specifically using tiles R108-T32TLS, R065-T32TMS, and R065-T32TNS (Fig. 1), at 10 m resolution. This yields an average of 21 SCAF observations per glacier in total over the period 2015-2021.

To model glacier mass balance, we force our model (cf. Sect. 3.2) with daily, gridded products provided by MeteoSwiss at a resolution of ca. 2 km. More specifically, we use daily mean temperature (T), precipitation sum (P), and daily mean incoming shortwave radiation (G) over our domain of interest (MeteoSwiss, 2018, 2021a, b).

The glacier geometry is defined using the glacier outlines provided by the SGI2016 (Linsbauer et al., 2021) and the SwissALTI3D DEM (swisstopo, 2020). To account for temporal changes in glacier area, we apply a simple volume-area



scaling relation, validated using area-change observations (see Sect. 3.2.2). The SGI2016 also provides information about the
100 debris-covered area for each glacier, which is used with the debris melt factors provided by Rounce et al. (2021) to account for
the effect of supraglacial debris cover on mass balance (see Sect. 3.2.1).

For validation, the model outputs are compared against (i) seasonal glacier-specific mass balance inferred from direct mea-
surements for 23 glaciers, included in the GLAMOS long-term monitoring programme (Huss et al., 2015; GLAMOS, 2024a),
and (ii) daily to monthly point mass balance measurements available for 19 glaciers from repeated field measurements during
105 the summer spanning periods of 7-90 days (GLAMOS, 2024b).

3 Methods

To provide daily mass balance estimates for every glacier in the Swiss Alps from 2010 to 2024, we follow the concept proposed
by Cremona et al. (2025). The approach separates the accumulation and ablation components of the modelled mass balance by
relying on geodetic ice volume changes and SCAF observations.

3.1 Ice volume changes

Changes in ice volume are derived using the geodetic method, which relies on differentiating DEMs of a glacier captured at
different points in time to measure changes in surface elevation. The procedure for determining ice volume changes, while
based on the same underlying concept for both SNFI and swisstopo DEMs, exhibits some variations to account for DEM-
specific characteristics derived from the respective processing chain during DEM generation.

115 For the SNFI DEMs, we differentiate pairs of DEMs and derive the change in surface elevation over the glacier area by
masking the glacier extent with the outlines provided by the Swiss Glacier Inventory 2016 (SGI2016, Linsbauer et al. (2021)).
Note that we derive ice volume changes only for pairs of DEMs that are more than five years apart to reduce uncertainties due to
firm densification processes (Huss, 2013). After differentiating two DEMs, the difference of DEMs (DoD) is derived. However,
the DoD from these DEMs contains data gaps and outliers resulting from cloud cover in the stereo images or correlation issues
120 during DEM generation. To filter outliers, we divide the DoD into 20 m elevation bands according to a reference DEM, and
for each band, we filter values that are more than one standard deviation apart from the mean elevation change of the band.
Then, data gaps are filled following a hypsometric approach as implemented in the Python package xDEM (xdem contributors,
2021; Mannerfelt et al., 2022). This approach relies on the correlation between elevation and elevation change to capture
the hypsometric signal of each glacier. To minimise uncertainties introduced by the interpolation approach, DoDs with voids
125 exceeding 50% of the glacier area are excluded. From the interpolated and filtered DoDs, the ice volume change is calculated
by summing the values in the DoD.

Ice volume changes from the swisstopo DEMs (see GLAMOS, 2024d) were computed following a similar procedure, but
with two main differences. (1) The temporally closest glacier outline to each of the two DEMs to be compared used to define
glacier area and the perimeter used for evaluating surface elevation change. In addition to the SGI2016, outlines are available
130 for most glaciers are available at 3- to 6-year intervals, for some glaciers even at 1-year intervals. (2) Unlike the SNFI DEMs,



the swisstopo DEMs are delivered free of voids, and outliers have already been filtered during DEM generation. Therefore, the outlier filtering step and the gap filling step described above were not necessary. However, in some cases, the exact daily period of these ice volume change observations could not be resolved exactly as the acquisition dates of the actual DEM data were not traceable and only the year the DEM was known. To address this, the missing dates of these DEMs are aligned with those from the SNFI DEMs since both datasets are based on the same aerial imagery (see Section 2). Therefore, when only one DEM is available for a given year, we assign it the same date as the SNFI DEM for that year. In years with multiple DEMs from different acquisition dates, the mean acquisition date of the SNFI DEMs for that year is taken, whereby the standard deviation in the acquisition date indicates the temporal spread of the DEMs within that year. Ice volume changes with lower standard deviations in acquisition dates are favoured to reduce uncertainties and improve the temporal constraint on the time period for ice volume changes based on swisstopo DEMs (GLAMOS, 2024d).

As a result, for each glacier, we obtain multiple estimates of the ice volume change over the study period, which are used during model calibration. For Grosser Aletschgletscher (Fig. 2), taken here as an explanatory example, seven estimates of the ice volume change are available within the period 2006–2023, covering different years. Three of these estimates are derived from SNFI DEMs and four from swisstopo DEMs. Each of the seven geodetic ice volume changes is used during calibration in an ensemble approach, meaning that for Grosser Aletschgletscher, the ensemble consists of seven parameter sets (see Sect. 3.2.3). Across the 1400 Swiss glaciers, the number of geodetic ice volume change estimates per glacier ranges from 0–38, with an average of eight evaluated periods per glacier.

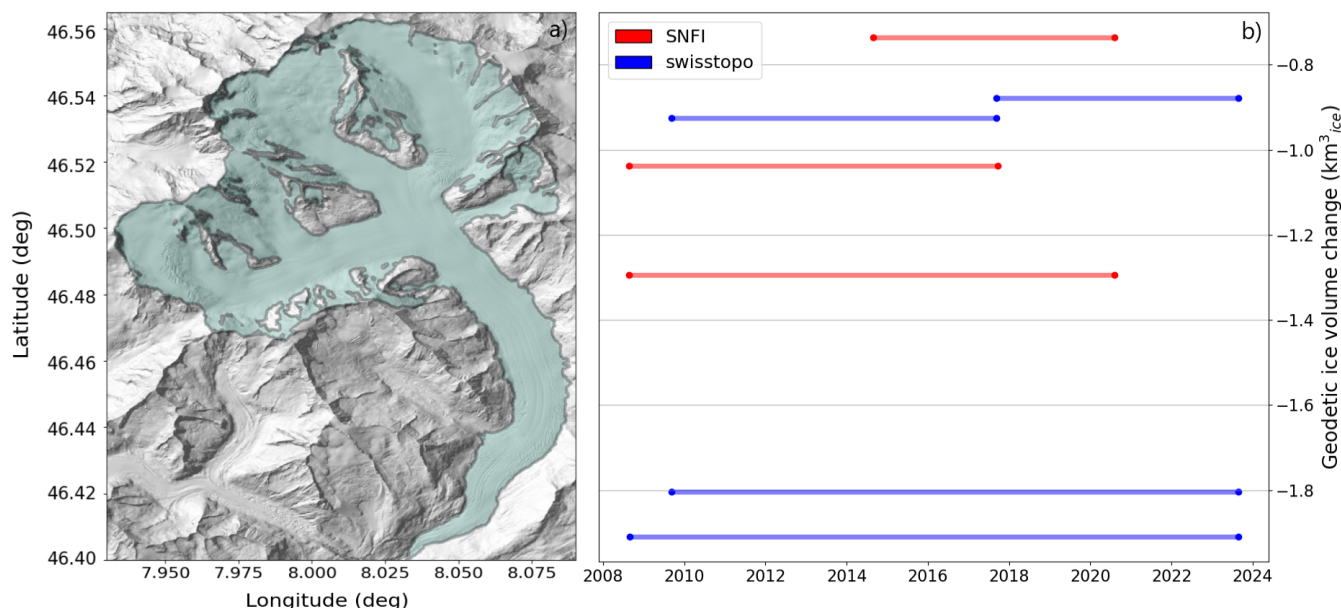


Figure 2. Temporal coverage of the geodetic ice volume changes available for Grosser Aletschgletscher. a) Overview of Grosser Aletschgletscher with glacier outline from the SGI2016. b) Geodetic ice volume change based on the SNFI DEMs (red) and swisstopo DEMs (blue).



3.2 Mass balance modelling

We model the altitudinal distribution of glacier surface mass balance using CRAMPON (Cryospheric Monitoring and Prediction Online, Landmann et al., 2021), with a very similar setup as presented in Cremona et al. (2025). CRAMPON is an operational mass balance model for calculating glacier-specific mass balance on a daily scale. The model discretises a glacier into elevation bands of 20 m and for each elevation band snow accumulation and ice/snow melt is computed. Accumulation is modelled according to the concept proposed by Huss et al. (2008):

$$c_{\text{sfc}}(z) = c_{\text{prec}} \cdot P \cdot \left[1 + (z - z_{\text{ref}}) \cdot \frac{\partial P}{\partial z} \right], \quad (1)$$

where $c_{\text{sfc}}(z)$ is the snow accumulation (m w.e.d^{-1}) at elevation z , c_{prec} is the precipitation correction factor, P is the sum of solid precipitation at the reference elevation z_{ref} , and $\frac{\partial P}{\partial z}$ is a precipitation gradient.

To model ablation, two different melt model formulations by Hock (1999) and Pellicciotti et al. (2005) are employed. Melt in the Hock model is determined as follows:

$$a_{\text{sfc}}(z) = (\text{MF} + a_{\text{snow/ice}} \cdot I_{\text{pot}}(z)) \cdot \max(T(z) - T_{\text{melt}}, 0), \quad (2)$$

where MF is the temperature melt factor ($\text{m w.e.K}^{-1} \text{d}^{-1}$), $a_{\text{snow/ice}}$ are two radiation factors for snow and ice ($\text{m w.e.m}^{-2} \text{d}^{-1} \text{W}^{-1} \text{K}^{-1}$) and $I_{\text{pot}}(z)$ is the potential clear-sky direct solar radiation (W m^{-2}). We assume $T_{\text{melt}} = 0^\circ \text{C}$, and a ratio $a_{\text{snow}}/a_{\text{ice}}$ of 0.75 (Hock, 1999; Farinotti et al., 2012). Melt in the Pellicciotti model is determined as follows:

$$a_{\text{sfc}}(z) = \begin{cases} \text{TF} \cdot T(z) + \text{SRF} \cdot (1 - \alpha(z)) \cdot G(z) & \text{if } T(z) > T_{\text{melt}} \\ 0 & \text{if } T(z) \leq T_{\text{melt}}, \end{cases} \quad (3)$$

where TF is the temperature factor ($\text{m w.e.K}^{-1} \text{d}^{-1}$), SRF is the shortwave radiation factor ($\text{m}^3 \text{d}^{-1} \text{W}^{-1}$), $\alpha(z)$ is the albedo (W m^{-2}) parametrized following Brock et al. (2000), and $G(z)$ is the incoming shortwave radiation (W m^{-2}). Note that for this model, $T_{\text{melt}} = 1^\circ \text{C}$ (Pellicciotti et al., 2005). We then combine the outputs of the two melt models by taking the average of the computed daily melt. The temperature at each elevation band ($T(z)$) in Eqs. (2) and (3) is derived as follows:

$$T(z) = T \cdot (z - z_{\text{ref}}) \cdot \frac{\partial T}{\partial z}, \quad (4)$$

where T is the temperature at the reference elevation z_{ref} of the grid cell in the meteorological product closest to the glacier centroid, and $\frac{\partial T}{\partial z}$ is the temperature lapse rate derived from temperature values of the surrounding cells.

3.2.1 Debris cover

Supraglacial debris cover has a significant effect on melt enhancement or reduction for the ice underneath (Nicholson and Benn, 2012; Rounce et al., 2021). To account for this effect, the modelled melt resulting from Eqs. (2) and (3) is scaled with a



debris melt factor. A debris melt factor below 1 indicates that the debris protects the ice, leading to reduced melt as compared to clean ice. This is often the case for a thick layer of debris with a significant isolation effect on the underlying ice. Vice versa, a debris melt factor above 1 indicates enhanced melt compared to clean ice, which is typical for a thin layer of debris that offers virtually no isolation effect but decreases the surface albedo. For glaciers larger than 2 km², we use the melt factor provided by Rounce et al. (2021), which is derived relying on Landsat-8 images spanning 2013-2018, thus it is aligned with the study period. At each elevation band, the average debris melt factor is calculated and multiplied with the modelled melt from Eqs. (2) and (3), but only if the elevation band is snow-free. For the smaller glaciers, Rounce et al. (2021) did not calculate the debris enhancement factor. For these glaciers, we derive the average melt factor for each elevation band by using the debris-covered area provided by the SGI2016 and assuming a debris melt factor of 0.63, i.e. the mean value found by Rounce et al. (2021). In this approach, debris coverage is kept constant over the study period, i.e. it does not evolve over time.

3.2.2 Glacier area evolution

To model the evolution of the glacier area over the study period, we employ the approach proposed by Möller and Schneider (2010). The approach relies on the volume-area scaling law (Bahr et al., 1997), which relates the volume and the area of a glacier with a power law as:

$$V = c \cdot A^\gamma, \quad (5)$$

where V is the glacier volume, A the glacier area, γ a dimensionless scaling exponent, and c a scaling coefficient. Möller and Schneider (2010) apply the volume-area scaling law to relate changes in glacier volume and area. Following this concept, the glacier area at the end of every year is updated as follows:

$$A_{y+1} = \left(\frac{V_y + \Delta V_y}{c} \right)^{\frac{1}{\gamma}}, \quad (6)$$

where V_y is glacier volume at the end of the previous year, ΔV_y is the volume change over the current year, and γ and c are the scaling exponent and coefficient as in Eq. (5). We use Eq. (6) to infer evolving glacier area with $\gamma=1.36$ according to the literature (Bahr et al., 2015), and directly defining c with the glacier-specific area and volume known for the year of the SGI2016 (Linsbauer et al., 2021; Grab et al., 2021). Since the area and volume for the inventory date are given, this year serves as our starting point for the simulations. We then update the glacier area forward in time (up to 2024) and backwards (back to 2010) by first calculating the cumulative yearly mass balance with Eqs. (1)-(3), which allows deriving the ΔV_y , and subsequently calculating the glacier area with Eq. (6) at the next time step. To update the area-elevation distribution of our model domain, it is assumed that all changes in glacier area occur in the ablation zone by attributing relative annual area changes equally to all bands below the mean equilibrium line altitude.



3.2.3 Model calibration

The mass balance model is calibrated relying on the concept described in Cremona et al. (2025), i.e. by combining information from SCAF observations and geodetic ice volume changes with a three-step optimisation procedure (Fig. 3). In the first step, the melt parameters (MF and $a_{\text{snow/ice}}$ in Eq. (2), and TF and SRF in Eq. (3)) are tuned to match the observed ice volume change. Here, a density of volume change of 900 kg m^{-3} is assumed to convert mass change to ice volume change. This assumption is motivated by the almost complete disappearance of firn areas observed since the beginning of the 21st century in the Swiss Alps, resulting in a rapid decline in the importance of firn processes in the investigated region. In the second step, the accumulation parameter, i.e. c_{prec} in Eq. (1), is tuned to minimise the difference between modelled and observed SCAFs over the melt seasons 2015-2021, i.e. the value of c_{prec} with the lowest Root Mean Square Error (RMSE) is selected (for more details refer to Cremona et al. (2025)). In the third step, the temperature lapse rate is adjusted to further optimise the model's reproduction of the observed SCAF. This step is new with respect to the procedure presented in Cremona et al. (2025), and it addresses the significant impact of the temperature lapse rate on the altitudinal distribution of mass balance and, hence, on the modelled course of the SCAF during the melt season. The initial estimate of the temperature lapse rate is computed from the gridded temperature data, deriving the lapse rate from the temperature and elevation of the cells next to the glacier. This provides insights into the lapse rate for a wider area but neglects local patterns. We then refine this estimate by adjusting it in 5% increments, selecting the value that minimises the difference between modelled and observed SCAFs.

This procedure is applied for every value of the ice volume change available from the swisstopo DEMs (GLAMOS, 2024d) and the ones derived in this study from the SNFI DEMs, resulting in one parameter set for each value of a geodetic ice volume change inferred over various periods of at least five years between 2010 and 2024, whereby parameters remain constant over the study period. Across the 87 glaciers where this calibration approach is applied, the number of parameter sets ranges from 1-20, with an average of 5 parameter sets per glacier. For each parameter set, the daily mass balance over 2010-2024 is calculated, i.e. in an ensemble approach, whereby the final estimate for the daily mass balance corresponds to the mean of the ensemble, and the standard deviation provides insights into the uncertainty. Note that this uncertainty only considers variations in the model outputs resulting from different geodetic volume changes used during calibration. This is the most influential factor, as noted by Cremona et al. (2025), but other sources of uncertainty are discussed in Section 4.4.

3.2.4 Extrapolation of parameters

A comprehensive quantitative assessment of regional mass balance requires reliable estimates of model parameters for all glaciers in the region. Therefore, the parameters derived for the 87 glaciers must be extrapolated to the rest of the Swiss glaciers. This extrapolation is done using machine learning, which is widely applied across earth sciences (Zhang et al., 2022), including several examples in glaciology (Bolibar et al., 2020; de Roda Husman et al., 2024; van der Meer et al., 2025), to capture spatio-temporal relations of environmental variables. In this study, we use eXtreme Gradient Boosting (XGBoost, Chen and Guestrin, 2016), a supervised-learning model consisting of an ensemble of decision trees that are built sequentially during training, and we aim to extrapolate the accumulation parameter c_{prec} across all Swiss glaciers. The attributes used for the extrapolation are

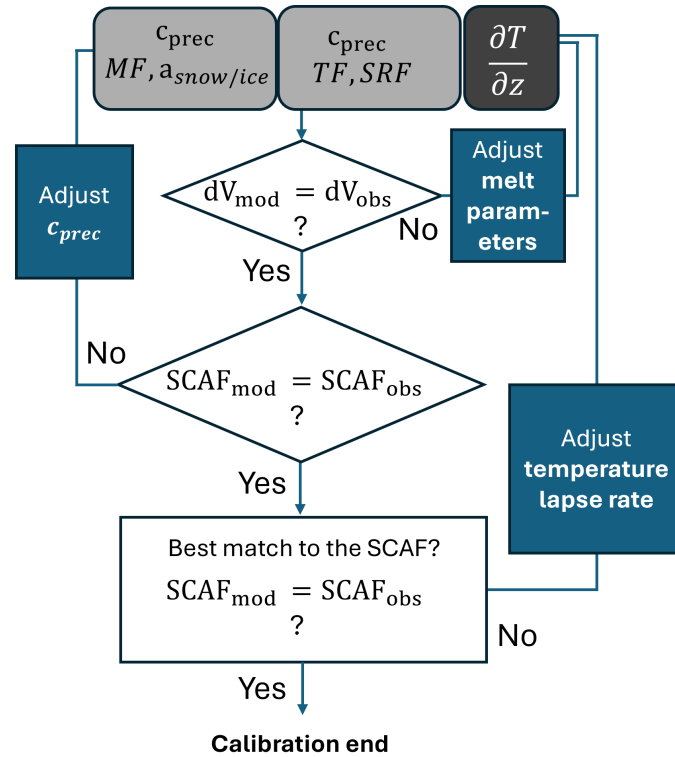


Figure 3. Three-step model calibration scheme. In the first step, the melt parameters (MF, $a_{\text{snow/ice}}$, TF, and SRF) are adjusted to match the observed ice volume change. In the second step, the precipitation correction factor (c_{prec}) is adjusted to optimise the reproduction of the observed SCAF over the melt seasons. In the third step, the temperature lapse rate is adjusted to further minimise differences between modelled and observed SCAF.

235 the geographic coordinates, i.e. the longitude and latitude of the glacier centroid, the median glacier elevation, the median glacier slope, the median glacier aspect, and the glacier area. These attributes are given in the SGI2016. The hyperparameter space of the XGBoost model is constrained by the maximum tree depth $\in [2, 8]$, the number of estimators $\in [10, 700]$, and the learning rate $\in [0.01, 0.3]$. To identify the best model, a randomised grid search with five-fold cross-validation over the hyperparameter space is performed, resulting in a model that reproduces c_{prec} with a cross-validation RMSE of 0.37 (-). This

240 model is employed to extrapolate c_{prec} to approximately 1300 glaciers. Afterwards, for each glacier, the melt parameters are tuned to match the ice volume changes. As before, multiple parameter sets result for each glacier, depending on the number of ice volume changes available, which are treated with an ensemble approach to provide daily mass balance estimates over the study period. The extrapolation enables us to provide daily mass balance estimates over 2010-2024 for 1344 glaciers (98% of the glacier area). For the remaining glaciers, for which no change in ice volume is available, the mass balance is assumed to be

245 equivalent to the average daily Swiss-wide mass balance.



3.3 Validation

To assess the uncertainty of our approach, the model outputs are compared against i) seasonal glacier-wide mass balance for individual glaciers inferred from direct measurements (GLAMOS, 2024a) and ii) weekly to monthly point mass balance measurements during the summer season available spanning a period of 7-90 days (GLAMOS, 2024b). Seasonal glacier-wide mass balance is validated on a subset of ten glaciers (Fig. 4) to evaluate the performance of the calibration relying on geodetic ice volume changes and SCAF observations (see Sect. 3.2.3). With a mean absolute deviation (MAD) of 0.27 m w.e and a bias of -0.08 m w.e the model slightly underestimates winter mass balance, and with a MAD of 0.36 m w.e and a bias of -0.05 m w.e the model provides slightly more negative annual mass balance. These values, together with the data points clustering along the 1:1 line in both cases (Fig. 4), demonstrate a good agreement with observed seasonal mass balances for glaciers calibrated on SCAF observations. Additionally, seasonal glacier-wide mass balance is validated against a second set of 13 glaciers, for which no SCAF observations are available and to which precipitation correction factors have been extrapolated (see Sect. 3.2.4). For these glaciers, the MAD for winter balance is 0.31 m w.e (bias of -0.02 m w.e), and the MAD for annual mass balance is 0.38 m w.e (bias of 0.16 m w.e). Despite a small bias towards less negative mass balances than observed, these values confirm the reliability of the extrapolation approach with machine learning. The validation against sub-seasonal point mass balance measurements included 19 glaciers, of which 10 relied on extrapolated precipitation correction factors. Validation against point measurements is conducted for shorter periods, i.e. up to the weekly scale, providing valuable insights into the accuracy of the model outputs on short time scales and thus the temporal course of modelled mass balance over the summer season. Although daily point measurements are available for some glaciers (Landmann et al., 2021; Cremona et al., 2023), we aggregated such measurements at the weekly scale to reduce measurement uncertainties. Because CRAMPON is an elevation-band type of model, we compare the observed mass balance acquired at the elevation z with the modelled mass balance resulting for the elevation band that includes the elevation z . The normalised mean absolute deviation (NMAD), calculated as the MAD between modelled and observed values divided by the observed values, is 33%, confirming the model reliability in providing daily point mass balances (Fig. 5).

4 Results and Discussion

4.1 Ice volume change over 2010-2024

According to our results, glaciers in the Swiss Alps lost $15.2 \pm 1.6 \text{ km}^3$ of ice over the period 2010-2024, i.e. almost 25% of their volume in 2010 (Fig. 6). This corresponds to an average yearly ice volume loss of 1 km^3 of ice. Yearly volume changes range from $-2.4 \pm 0.16 \text{ km}^3$ of ice (in 2022) to a slight volume gain of $+0.13 \pm 0.09 \text{ km}^3$ in 2014 (Fig 6 b). Other years with particularly large losses are 2011, 2017, and 2023, whereas years with only slightly negative mass balance are 2013 and 2021. The region with the largest volume losses over the study period is the Aletsch region, which contributed to almost 30% of the total ice volume loss in Switzerland. Such high losses for this region are a consequence of below-average annual mass balance (Fig. 7 b) combined with the large glacierized area in the region.

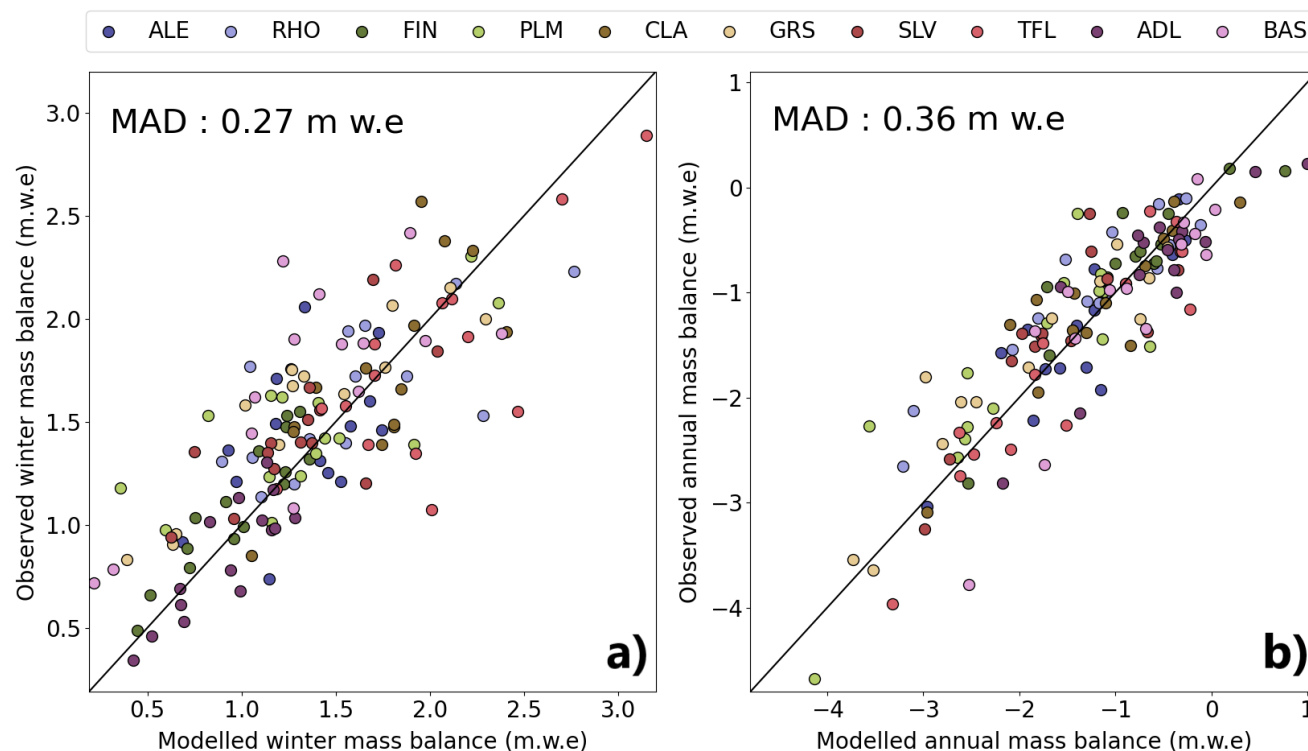


Figure 4. Validation of seasonal glacier-wide mass balance. a) Comparison between modelled and observed winter mass balance. b) Comparison between modelled and observed annual mass balance.

4.2 Seasonal mass balance and climatic drivers

The area-weighted average winter mass balance for the Swiss Alps during the period 2010-2024, taken as the cumulative mass balance between 1 October - 30 April, is 1.27 m w.e. Regional differences in the average winter mass balances are shown in Figure 7 a, where glacier-wide estimates are aggregated on a 20 x 20 km grid. The largest winter snow accumulation can be observed in central and western Switzerland, with values ranging between 1.5-1.9 m w.e. The Aletsch region and the Engadin align with the Swiss-wide average with values around 1.3 m w.e, and the lowest winter mass balances are observed in Valais with values of 0.9-1.2 m w.e. The area-weighted Swiss-wide average annual mass balance over the study period is -0.95 m w.e, and the aggregated values for the 20 x 20 km grid range between -0.6 and -1.5 m w.e (Fig. 7 b). Although winter balances correlate well in space, no clear pattern is revealed for the spatial variability of average annual mass balances, whereby neighbouring glaciers and regions present very different values. The only region with a clear signal is the Southern Valais, showing less negative values compared to the Swiss-wide average. This fact has previously been documented by several studies that showed the predominant effect of topographical characteristics on annual balance variations in space, such as the glaciers' mean elevation, as well as the slope, area, and aspect (Kuhn et al., 1985; Hoelzle et al., 2003; Huss et al., 2012; Fischer et al., 2015). Thus, several neighbouring regions in Figure 7 b), which may include glaciers with different topographical

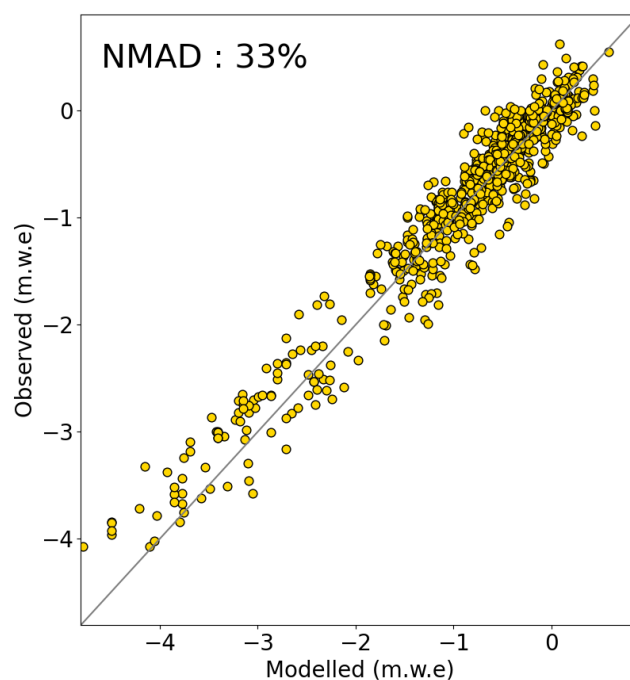


Figure 5. Validation of cumulated modelled daily mass balance against point mass balance measurements for periods spanning 7-90 days.

characteristics, present diverging average annual mass balances. In contrast, the high spatial correlation for winter balances in Figure 7 a) indicates that this variable shows a clear dependence on regional precipitation patterns, while strong topographical controls (e.g. snow redistribution by wind and avalanches) are relevant at the local to glacier scale.

295 Seasonal mass balances for individual years in the study period are investigated in more detail (Fig. 8), and are compared against temperature and precipitation patterns to further assess the importance of climatic drivers for determining spatio-temporal glacier mass balance variability across Switzerland (Fig. 9). This is achieved by computing seasonal mass balance anomalies for each year with respect to the average seasonal mass balance over the study period, and comparing them to the anomaly of (i) the total precipitation sum over the winter season (Oct - April) and (ii) the average temperature over summer
300 (May - Sept). Seasonal mass balance anomalies exhibit different regional signals over the years (Fig. 8), and notably, spatial differences in the anomalies across regions happen to be more accentuated for years with more heterogeneous precipitation distribution (Fig. 9). Furthermore, it can be observed that the spatial pattern in the mass balance variability remains consistent between winter and annual balance in most cases. This consideration is supported by the fact that precipitation anomalies are spatially much more heterogeneous than temperature anomalies and thus have a larger influence on spatial variations of mass
305 balance (Fig. 9). These factors together indicate that the year-to-year spatial variability of mass balance is strongly controlled by regional winter accumulation anomalies.

A quantitative comparison between mass balance anomalies and anomalies of the meteorological variables over the study period is shown in Figure 10. The anomaly of the winter precipitation sum correlates well with the winter mass balance anomaly

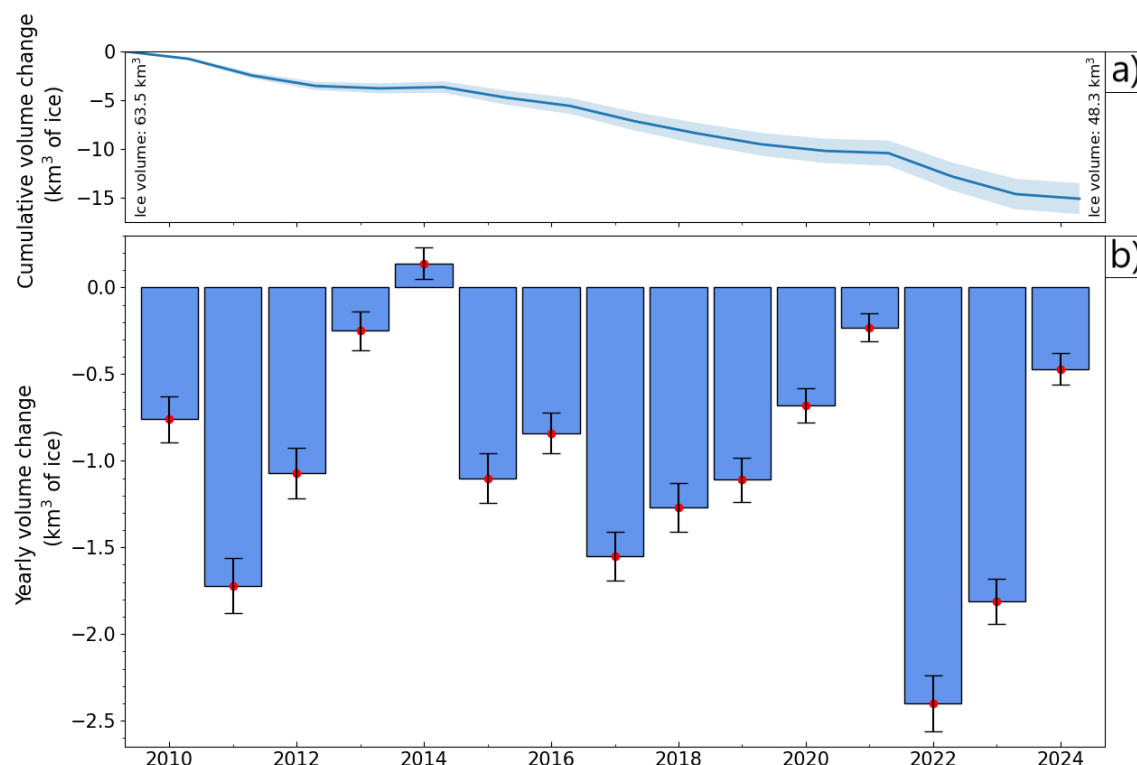


Figure 6. Swiss-wide ice volume change over 2010-2024. a) The cumulative ice volume change (blue line) over the study period is shown with the respective uncertainty (shaded area). b) Yearly volume changes (blue bars) with respective uncertainty ranges are shown.

($r = 0.86$), and the anomaly of the mean summer temperature correlates well with the summer mass balance ($r = -0.77$). The high correlations confirm the predominant influence of temperature and precipitation on determining seasonal mass balance variations. Nevertheless, the spread demonstrates the involvement of other processes, such as the effect of cloudiness and wind-driven turbulent heat exchange, or more localised snow redistribution by wind or avalanches and the influence of Saharan dust on snow albedo. These factors are known to have a significant influence on the balance of glacier mass (Gabbi et al., 2015; Freudiger et al., 2017; Rounce et al., 2021).

4.3 Short-term mass balance variability

Our approach has the advantage of providing mass balance estimates with a high spatio-temporal resolution for all glaciers of the Swiss Alps, enabling us to derive and compare daily mass balances across regions (Fig. 11). In Figure 11, the daily mass balance is aggregated over the four main hydrological basins in Switzerland (Rhine, Rhone, Po, and Danube), and it is compared for three years, i.e. a year with slightly positive mass balance (2014), an average year (2016), and a highly negative year (2022). In 2014, the mass balance at the end of the year is close to zero for the Rhine and Rhone basins, whereas it is more positive for the Po and Danube basins (Fig. 11 a). The lower summer temperatures recorded in 2014 across Switzerland, i.e. by

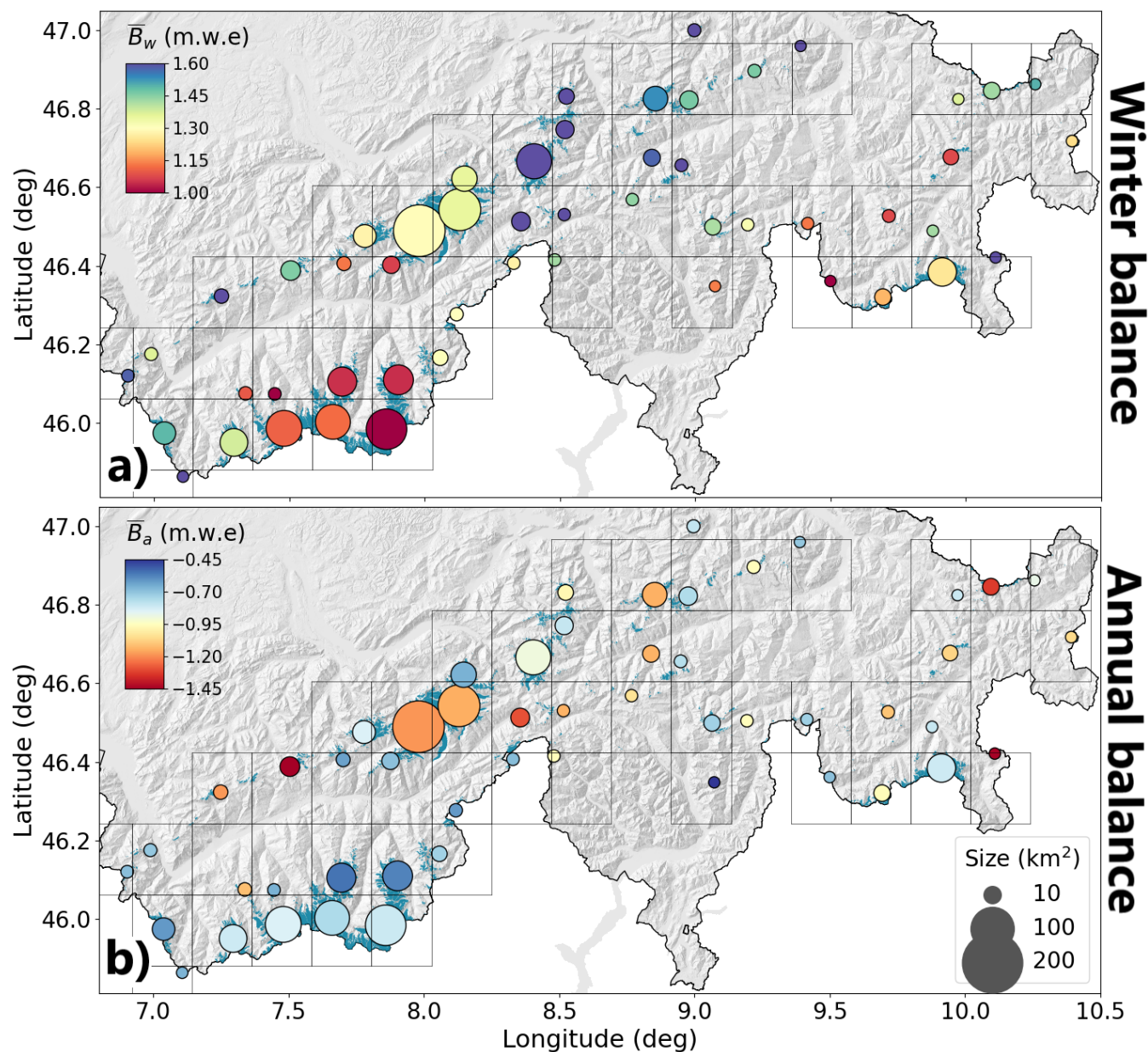


Figure 7. Average seasonal mass balance for the Swiss Alps over 2010-2024. (a) Average winter balance (30 April), and (b) average annual balance (30 Sept). Glacier-wide values are aggregated over a 20x20km grid with area-weighted averaging, whereby the size of the circles shows the glacierized area within each grid cell.

-1 to -1.5 °C with respect to the 2010-2024 average (Fig. 9 e.2), reflect the smaller melt rates observed across the four basins in 2014 compared to 2016 and 2022 (Fig. 11). Winter accumulation for 2014, instead, presents larger variations, which closely

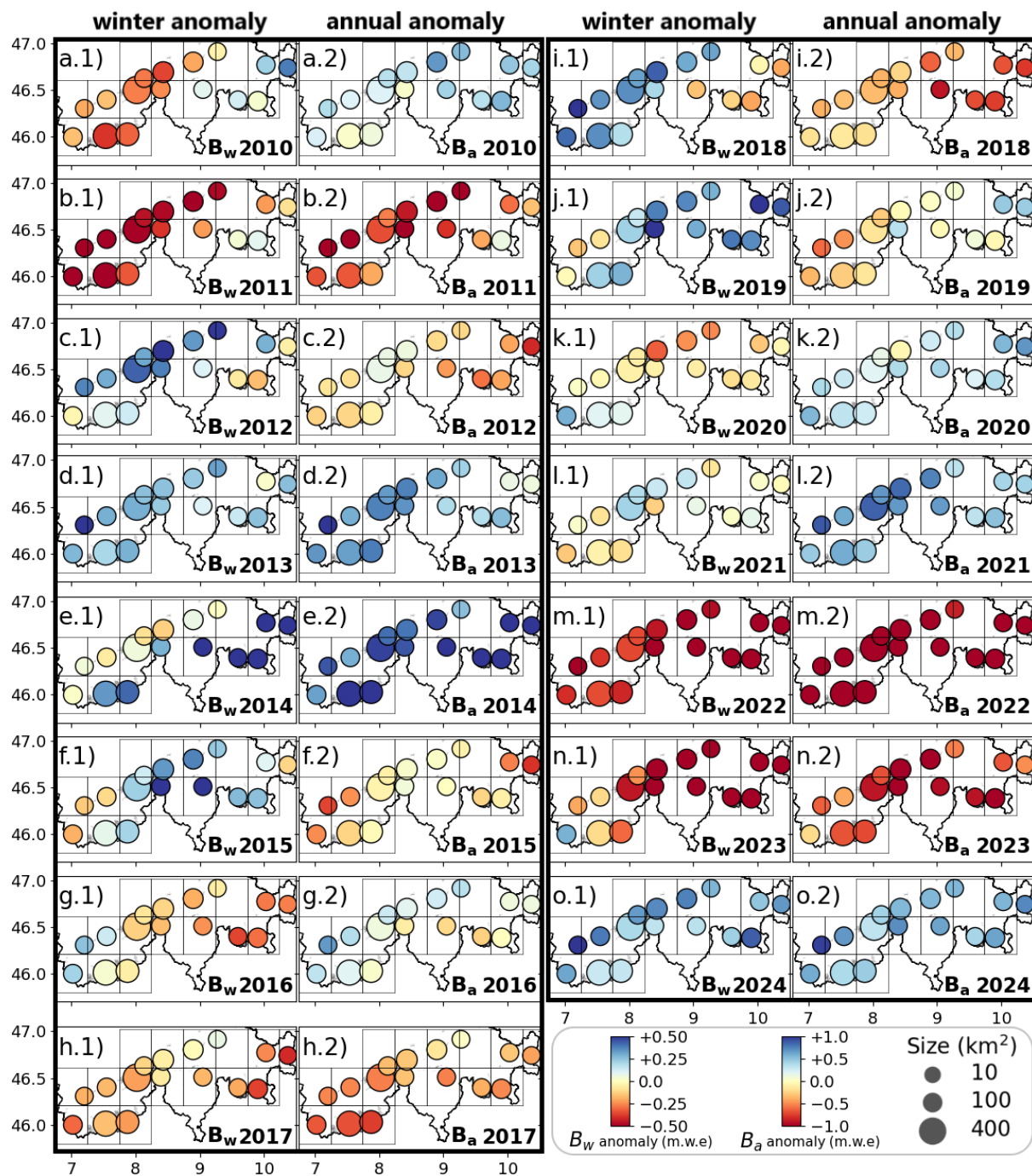


Figure 8. Anomaly of the winter (B_w) and annual (B_a) mass balance with respect to the average winter and annual mass balance over the study period for the years 2010-2024.

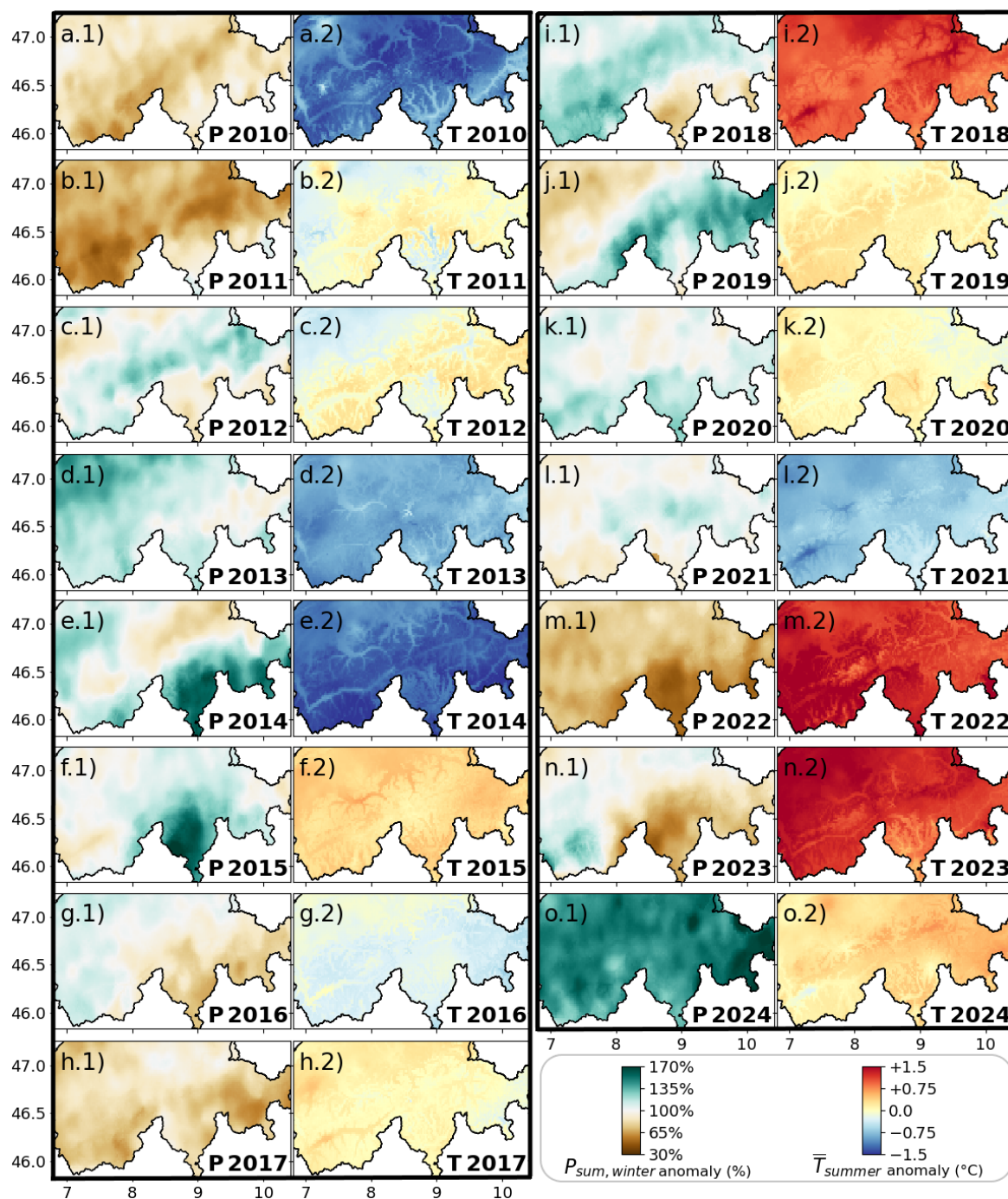


Figure 9. Anomaly of winter precipitation sum (Oct - April) and mean summer temperature (May - Sept) with respect to the average values over 2010-2024.

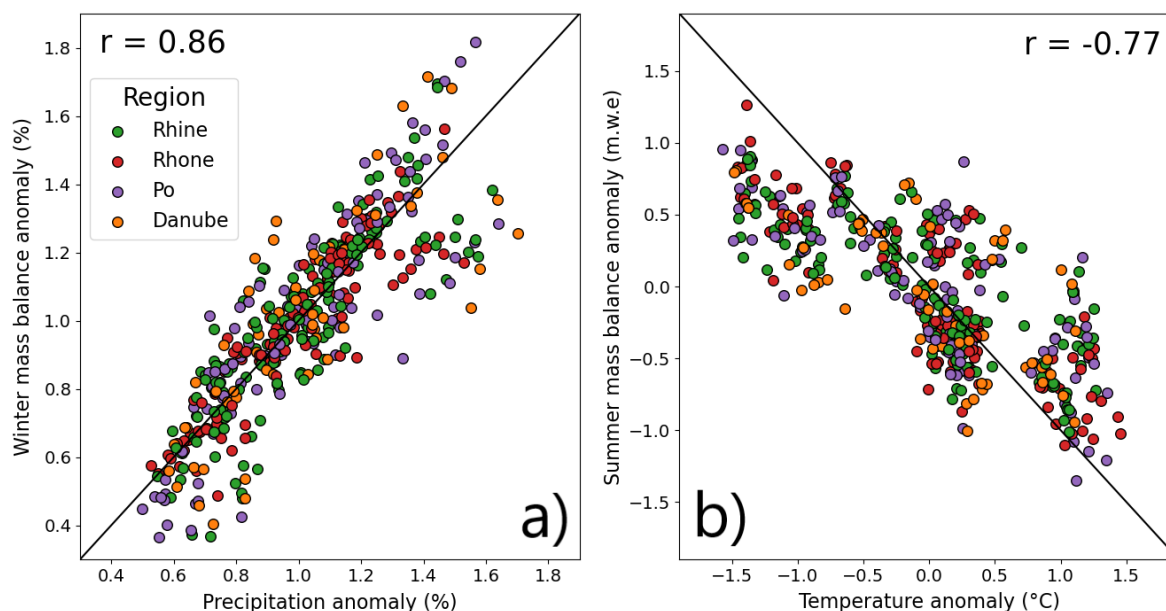


Figure 10. Correlation between mass balance anomalies and the anomalies in meteorological variables for all Swiss glaciers (aggregated on the 20 x 20 km grid). (a) Winter precipitation anomaly versus winter mass balance anomaly. b) Summer temperature anomaly versus summer mass balance. The colours distinguish the different hydrological basins where the glaciers are located.

match the spatial variability of the winter precipitation (Fig. 9 e.1). While the Rhine and Rhone basins experienced average
325 winter accumulation, the Po and Danube basins exhibited above-average accumulation, with winter mass balances of more
than 2 m w.e by the end of April. This difference is a key factor leading to slightly positive annual mass balances for the Po and
Danube basins in 2014. By comparing the course of the mass balance between 2014 and 2016, it can be observed that for the
Rhone and Rhone basins the winter accumulation is similar between the two years, and the higher melt rates in 2016 caused by
higher summer temperatures are mainly responsible for the more negative mass balance at the end of the year (−0.8 to −0.9 m
330 w.e). This highlights the importance of summer temperatures for driving annual mass losses. The comparison for the Po and
Danube basins between 2014 and 2016, instead, shows the impact of favourable conditions both during the winter and the
summer season on mass balance. With about twice the accumulation in 2014 and lower summer temperatures, the difference in
annual balance between 2014 and 2016 is of more than 1 m w.e. for both basins. On the contrary, the year 2022 demonstrates
the drastic effect of a year with extremely unfavourable conditions (Cremona et al., 2023; Voordendag et al., 2023; Berthier
335 et al., 2024). This year presented among the lowest winter precipitation sums recorded over most of Switzerland during the
study period, which combined with one of the warmest summers (Fig. 9), led to unprecedented ice losses recorded in one year,
i.e. with a mass balance of below -2 m w.e y^{-1} for all four basins (Fig. 11) and almost -2.5 km^3 of ice wastage for the Swiss
Alps (Fig. 6 b).

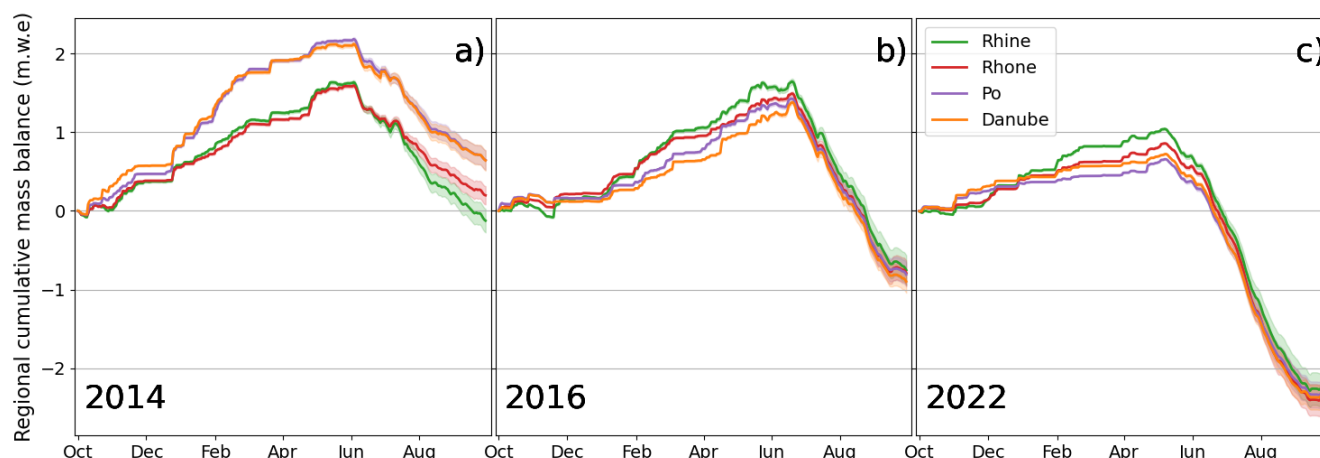


Figure 11. Comparison of daily regional mass balance aggregated over the four main hydrological basins in Switzerland, i.e. Rhine (in green), Rhone (in red), Po (in violet), and Danube (in orange), for three years, i.e. a positive year (2014, in panel a), an average year (2016, in panel b), and a negative year (2022, in panel c).

4.4 Comparison to existing approaches and limitations

340 The comparison between the results of this study based on distributed mass balance modelling constrained with SCAF obser-
vations and those obtained from statistically upscaling the seasonal variability (GLAMOS, 2024c; van Tiel et al., 2025)
generally reveals a high agreement, but also points out some differences (Fig. 12). The Swiss-wide volume change over the
study period agrees well for both approaches, with a difference in total volume change of approximately 10%, which is within
the respective uncertainty ranges. The volume losses found in the present study are slightly less negative. Despite the temporal
345 variations of annual volume changes agreeing well, the systematic difference between the two approaches can be observed in
most years, whereby larger differences are present in specific years (Fig. 12). The most prominent example is 2022 where our
results point to less important mass losses compared to extrapolating observed mass balances of that year. Large differences
are present also in 2014, 2023, and 2024. The differences between the two approaches in terms of total ice volume loss range
between 0.4 and 0.7 km³. Notably, all these years were characterised by non-average conditions, and in some cases, extreme
350 conditions. 2014 and 2024 experienced wet winter seasons, leading to large accumulation amounts, whereas 2022 and 2023
were among the warmest and driest years on record in Switzerland.

These differences are likely explained by three main factors. The first factor is linked with the methodological differences
between the two approaches. Here, we rely on glacier-specific modelling driven by daily meteorological data, in contrast with
the more data-driven approach relying on statistical upscaling of seasonal variability inferred from measurements for a subset
355 of about 20 glaciers (see also Dussaillant et al., 2025). Therefore, seasonal and annual mass balance variations are directly
determined by meteorological forcing and the optimally constrained model parameters in the present approach, while statistical
methods for inferring regional mass change extrapolate measured mass balance anomalies from a small set of observations.

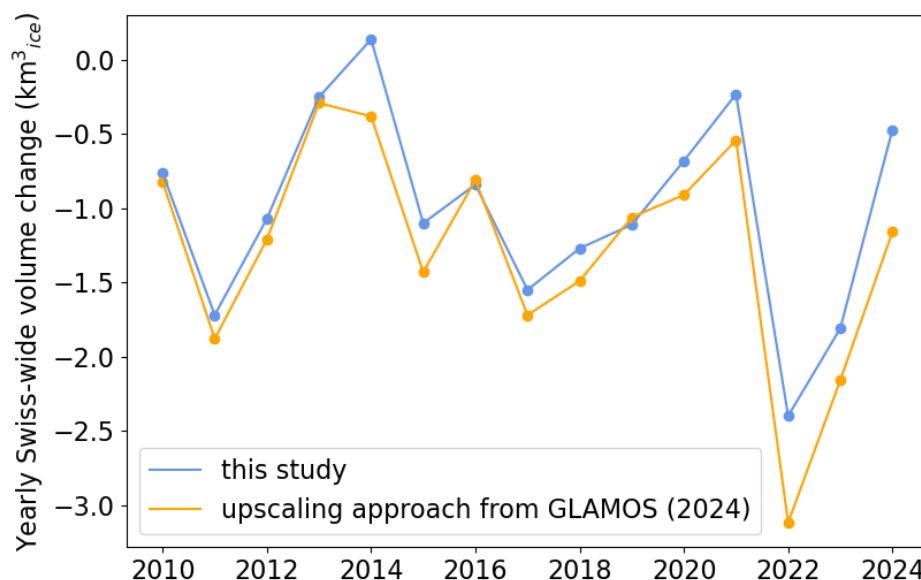


Figure 12. Comparison of the yearly Swiss-wide ice volume change between this study (blue) and the upscaling of local mass balance measurements (GLAMOS, 2024c; van Tiel et al., 2025) (orange).

The second factor is associated with the use of different input data. In the present study, we include newly-derived ice volume changes from a large set of digital elevation models covering the study period, while the statistical upscaling data product considered here (GLAMOS, 2024c; van Tiel et al., 2025) relied on longer-term and older geodetic mass balances (Fischer et al., 2015) for inferring glacier-specific mass change trends. This may be responsible for the systematic differences between the data sets.

The third factor is linked with the limitations and uncertainties of the respective approaches. A limitation of this study is that we assume a constant parameter set over the entire study period, neglecting temporal variations in the parameters that may be driven by processes not accounted for in the model. This, for example, pertains to the albedo effect of Saharan dust, or the influence of other components of the energy balance (e.g. turbulent heat fluxes, long-wave radiation variations). This can especially impact the temporal variability of mass balance and volume change, explaining some of the differences observed in individual years with non-average and even extreme conditions, i.e. in 2014, 2022, 2023, and 2024.

Despite this limitation impacting individual years, our approach has the advantage of relying on the most recent geodetic estimates. In addition, the high resolution of the results presented here, both in time and space, provides an elevation-specified distribution of daily mass balance, which is not available from direct upscaling of glacier mass balance observations. Furthermore, this study models mass balance for every glacier individually, relying on regional remote sensing products and machine learning for extrapolation; thus, estimates for glaciers without direct measurements are likely more reliable.

The uncertainties of modelled mass balance from our approach only account for differences in the geodetic ice volume changes used during calibration (see Sect. 3.2.3), as this is identified as the main impacting factor (Cremona et al., 2025).



Other uncertainty sources are those linked to (i) the modelled evolution of glacier area, (ii) the SCAF observations used during calibration, and (iii) extrapolation with machine learning. Cremona et al. (2025) investigated sources (i) and (ii) and reported a difference in the seasonal mass balance of 0.04 m w.e when comparing two scenarios with a difference of the yearly glacier area change of 0.5%. They also found the modelled mass balance to be far less sensitive to uncertainties in the SCAF observations as compared to geodetic ice volume changes during calibration. Additional uncertainties in this study impacting winter mass balance are those introduced by the extrapolation of the precipitation correction factor with machine learning. The machine learning algorithm provides precipitation correction factors with a cross-validation RMSE of 0.37 (see Sect. 3.2.4) and the winter mass balance with a MAD of 0.31 m w.e to the observed values (see Sect. 3.3). Considering that the Swiss-wide average precipitation correction factor is 1.8 and the winter mass balance 1.27 m w.e, uncertainties in winter mass balance introduced during the extrapolation correspond to 20-25% on average.

5 Conclusions

In this study, we provide the daily mass balance for the ~ 1400 glaciers in the Swiss Alps over the period 2010-2024. Relying on a modelling framework and exploiting machine learning techniques for spatial extrapolation, remote sensing observations of the snow-covered area fraction are combined with geodetic volume changes to separate the accumulation and ablation components and thus better reproduce the seasonal variability of mass balance.

We estimate a total ice volume change over 2010-2024 of $-15.2 \pm 1.6 \text{ km}^3$, i.e. almost 25% of the ice volume in 2010 was lost in 15 years. Swiss-wide seasonal average mass balances over the study period amount to 1.27 m w.e for winter and to -0.95 m w.e for the annual scale, respectively. The spatial variability of seasonal mass balance is further evaluated to capture regional differences, showing a clear spatial pattern for winter accumulation with the highest amounts in central and western Switzerland ranging between 1.5-1.9 m w.e and lowest values are recorded in Valais with values of 0.9-1.2 m w.e. Winter accumulation exhibits high spatial correlation, revealing a strong dependence on precipitation patterns, whereas annual balances ranging between -0.6 and -1.5 m w.e are less spatially correlated, confirming the predominant effect of local topographical factors on annual balance as already documented in the literature.

The high spatio-temporal resolution of our approach enabled us to better understand the relation between seasonal mass balance and the climatic drivers in the Swiss Alps, underlining the relevance of winter accumulation on the year-to-year spatial variability of mass balance. Furthermore, this study highlights the importance of remote sensing observations to provide reliable estimates of short-term mass balance of unmeasured glaciers at the scale of entire regions. This suggests that observations of the snow-covered area fraction on glaciers may improve glacier-specific modelling at the large scale.

Code and data availability. The model code is available at <https://github.com/acremona/crampon> (a DOI will be assigned upon publication). The modelled daily mass balance will be made available in an online repository upon publication.



Author contributions. AC, MH, DF, and JML conceived the study. MM, JML, and CG processed and derived the SNFI DEMs. MH derived geodetic ice volume changes from swisstopo DEMs, and AC derived the geodetic ice volume changes from SNFI DEMs. MVDM provided support to AC on the machine learning algorithm. AC conducted the modelling, supported by MH, JML, and DF. AC wrote the paper and produced the figures, with contributions from all co-authors.

410 *Competing interests.* At least one of the (co-)authors is a member of the editorial board of The Cryosphere. The authors have no other competing interests to declare.

Acknowledgements. This study is supported by the project 'Machine Learning aided Forecasting of drought related eXtremes (MaLeFiX)', conducted in the frame of the programme 'eXtremes' of the Swiss Federal Institute for Forest, Snow and Landscape Research (WSL). We are further grateful to the Swiss Federal Office of Topography (swisstopo) for the data contribution and collaboration within the GLAMOS
415 monitoring programme.



References

- Anghileri, D., Botter, M., Castelletti, A., Weigt, H., and Burlando, P.: A comparative assessment of the impact of climate change and energy policies on Alpine hydropower, *Water Resources Research*, 54, 9144–9161, <https://doi.org/10.1029/2017WR022289>, 2018.
- Bahr, D. B., Meier, M. F., and Peckham, S. D.: The physical basis of glacier volume-area scaling, *Journal of Geophysical Research: Solid Earth*, 102, 20 355–20 362, <https://doi.org/10.1029/97JB01696>, 1997.
- Bahr, D. B., Pfeffer, W. T., and Kaser, G.: A review of volume-area scaling of glaciers, *Reviews of Geophysics*, 53, 95–140, <https://doi.org/10.1002/2014RG000470>, 2015.
- Barandun, M., Huss, M., Usabaliev, R., Azisov, E., Berthier, E., Kääb, A., Bolch, T., and Hoelzle, M.: Multi-decadal mass balance series of three Kyrgyz glaciers inferred from modelling constrained with repeated snow line observations, *The Cryosphere*, 12, 1899–1919, <https://doi.org/10.5194/tc-12-1899-2018>, 2018.
- Barandun, M., Pohl, E., Naegeli, K., McNabb, R., Huss, M., Berthier, E., Saks, T., and Hoelzle, M.: Hot spots of glacier mass balance variability in Central Asia, *Geophysical Research Letters*, 48, e2020GL092 084, <https://doi.org/10.1029/2020GL092084>, 2021.
- Beraud, L., Cusicanqui, D., Rabatel, A., Brun, F., Vincent, C., and Six, D.: Glacier-wide seasonal and annual geodetic mass balances from Pléiades stereo images: application to the Glacier d’Argentière, French Alps, *Journal of Glaciology*, 69, 525–537, <https://doi.org/10.1017/jog.2022.79>, 2023.
- Berthier, E., Vincent, C., and Six, D.: Exceptional thinning through the entire altitudinal range of Mont-Blanc glaciers during the 2021/22 mass balance year, *Journal of Glaciology*, 70, e30, <https://doi.org/10.1017/jog.2023.100>, 2024.
- Bolibar, J., Rabatel, A., Gouttevin, I., and Galiez, C.: A deep learning reconstruction of mass balance series for all glaciers in the French Alps: 1967–2015, *Earth System Science Data*, 12, 1973–1983, <https://doi.org/10.5194/essd-12-1973-2020>, 2020.
- Brock, B. W., Willis, I. C., and Sharp, M. J.: Measurement and parameterization of albedo variations at Haut Glacier d’Arolla, Switzerland, *Journal of Glaciology*, 46, 675–688, <https://doi.org/10.3189/172756500781832675>, 2000.
- Chen, T. and Guestrin, C.: Xgboost: A scalable tree boosting system, in: *Proceedings of the 22nd ACM SIGKDD international conference on knowledge discovery and data mining, KDD ’16*, pp. 785–794, <https://doi.org/10.1145/2939672.2939785>, 2016.
- Compagno, L., Eggs, S., Huss, M., Zekollari, H., and Farinotti, D.: Brief communication: Do 1.0, 1.5, or 2.0° C matter for the future evolution of Alpine glaciers?, *The Cryosphere*, 15, 2593–2599, <https://doi.org/10.5194/tc-15-2593-2021>, 2021.
- Cremona, A., Huss, M., Landmann, J. M., Borner, J., and Farinotti, D.: European heat waves 2022: contribution to extreme glacier melt in Switzerland inferred from automated ablation readings, *The Cryosphere*, 17, 1895–1912, 2023.
- Cremona, A., Huss, M., Landmann, J. M., Schwaizer, G., Paul, F., and Farinotti, D.: Constraining sub-seasonal glacier mass balance in the Swiss Alps using Sentinel-2-derived snow-cover observations, *Journal of Glaciology*, 71, e25, <https://doi.org/10.1017/jog.2025.1>, 2025.
- de Roda Husman, S., Lhermitte, S., Bolibar, J., Izeboud, M., Hu, Z., Shukla, S., van der Meer, M., Long, D., and Wouters, B.: A high-resolution record of surface melt on Antarctic ice shelves using multi-source remote sensing data and deep learning, *Remote Sensing of Environment*, 301, 113 950, <https://doi.org/10.1016/j.rse.2023.113950>, 2024.
- Denzinger, F., Machguth, H., Barandun, M., Berthier, E., Girod, L., Kronenberg, M., Usabaliev, R., and Hoelzle, M.: Geodetic mass balance of Abramov Glacier from 1975 to 2015, *Journal of Glaciology*, 67, 331–342, <https://doi.org/10.1017/jog.2020.108>, 2021.
- Dumont, M., Monteiro, D., Filhol, S., Gascoin, S., Marty, C., Hagenmuller, P., Morin, S., Choler, P., and Thuiller, W.: The European Alps in a changing climate: physical trends and impacts, *Comptes Rendus. Géoscience*, 357, 25–42, <https://doi.org/10.5802/crgeos.288>, 2025.



- Dussaillant, I., Berthier, E., and Brun, F.: Geodetic mass balance of the Northern Patagonian Icefield from 2000 to 2012 using two independent methods, *Frontiers in Earth Science*, 6, 8, <https://doi.org/10.3389/feart.2018.00008>, 2018.
- Dussaillant, I., Hugonnet, R., Huss, M., Berthier, E., Bannwart, J., Paul, F., and Zemp, M.: Annual mass change of the world's glaciers from 1976 to 2024 by temporal downscaling of satellite data with in situ observations, *Earth System Science Data*, 17, 1977–2006, <https://doi.org/10.5194/essd-17-1977-2025>, 2025.
- Elsberg, D., Harrison, W., Echelmeyer, K., and Krimmel, R.: Quantifying the effects of climate and surface change on glacier mass balance, *Journal of Glaciology*, 47, 649–658, <https://doi.org/10.3189/172756501781831783>, 2001.
- Farinotti, D., Usselman, S., Huss, M., Bauder, A., and Funk, M.: Runoff evolution in the Swiss Alps: Projections for selected high-alpine catchments based on ENSEMBLES scenarios, *Hydrological Processes*, 26, 1909–1924, <https://doi.org/10.1002/hyp.8276>, 2012.
- Farinotti, D., Pistocchi, A., and Huss, M.: From dwindling ice to headwater lakes: could dams replace glaciers in the European Alps?, *Environmental Research Letters*, 11, 054 022, <https://doi.org/10.1088/1748-9326/11/5/054022>, 2016.
- Finger, D., Pellicciotti, F., Konz, M., Rimkus, S., and Burlando, P.: The value of glacier mass balance, satellite snow cover images, and hourly discharge for improving the performance of a physically based distributed hydrological model, *Water resources research*, 47, <https://doi.org/10.1029/2010WR009824>, 2011.
- Fischer, M., Huss, M., and Hoelzle, M.: Surface elevation and mass changes of all Swiss glaciers 1980–2010, *The Cryosphere*, 9, 525–540, <https://doi.org/10.5194/tc-9-525-2015>, 2015.
- Freudiger, D., Kohn, I., Seibert, J., Stahl, K., and Weiler, M.: Snow redistribution for the hydrological modeling of alpine catchments, *Wiley Interdisciplinary Reviews: Water*, 4, e1232, <https://doi.org/10.1002/wat2.1232>, 2017.
- Gabbi, J., Carenzo, M., Pellicciotti, F., Bauder, A., and Funk, M.: A comparison of empirical and physically based glacier surface melt models for long-term simulations of glacier response, *Journal of Glaciology*, 60, 1140–1154, <https://doi.org/10.3189/2014JG14J011>, 2014.
- Gabbi, J., Huss, M., Bauder, A., Cao, F., and Schwikowski, M.: The impact of Saharan dust and black carbon on albedo and long-term mass balance of an Alpine glacier, *The Cryosphere*, 9, 1385–1400, <https://doi.org/10.5194/tc-9-1385-2015>, 2015.
- Ginzler, C. and Hobi, M. L.: Countrywide stereo-image matching for updating digital surface models in the framework of the Swiss National Forest Inventory, *Remote Sensing*, 7, 4343–4370, <https://doi.org/10.3390/rs70404343>, 2015.
- GLAMOS: Swiss Glacier Mass Balance, release 2024, Glacier Monitoring Switzerland, <https://doi.org/10.18750/massbalance.2024.r2024>, 2024a.
- GLAMOS: Swiss Glacier Point Mass Balance Observations, release 2024, Glacier Monitoring Switzerland, <https://doi.org/10.18750/massbalance.point.2024.r2024>, 2024b.
- GLAMOS: Swisswide Glacier Mass Balance, release 2024, Glacier Monitoring Switzerland, <https://doi.org/10.18750/massbalance.swisswide.2024.r2024>, 2024c.
- GLAMOS: Swiss Glacier Volume Change, release 2024, Glacier Monitoring Switzerland, <https://doi.org/10.18750/volumechange.2024.r2024>, 2024d.
- Grab, M., Mattea, E., Bauder, A., Huss, M., Rabenstein, L., Hodel, E., Linsbauer, A., Langhammer, L., Schmid, L., Church, G., Hellmann, S., Déléze, K., Schaer, P., Lathion, P., Farinotti, D., and Maurer, H.: Ice thickness distribution of all Swiss glaciers based on extended ground-penetrating radar data and glaciological modeling, *Journal of Glaciology*, 67, 1074–1092, <https://doi.org/10.1017/jog.2021.55>, 2021.
- Hock, R.: A distributed temperature-index ice-and snowmelt model including potential direct solar radiation, *Journal of Glaciology*, 45, 101–111, <https://doi.org/10.3189/S0022143000003087>, 1999.



- 490 Hock, R., Kootstra, D.-S., Reijmer, C., et al.: Deriving glacier mass balance from accumulation area ratio on Storglaciären, Sweden., IAHS-AISH publication, pp. 163–170, 2007.
- Hock, R., Bliss, A., Marzeion, B., Giesen, R. H., Hirabayashi, Y., Huss, M., Radić, V., and Slangen, A. B.: GlacierMIP—A model intercomparison of global-scale glacier mass-balance models and projections, *Journal of Glaciology*, 65, 453–467, <https://doi.org/10.1017/jog.2019.22>, 2019.
- 495 Hoelzle, M., Haeberli, W., Dischl, M., and Peschke, W.: Secular glacier mass balances derived from cumulative glacier length changes, *Global and Planetary Change*, 36, 295–306, [https://doi.org/10.1016/S0921-8181\(02\)00223-0](https://doi.org/10.1016/S0921-8181(02)00223-0), 2003.
- Hugonnet, R., McNabb, R., Berthier, E., Menounos, B., Nuth, C., Girod, L., Farinotti, D., Huss, M., Dussailant, I., Brun, F., et al.: Accelerated global glacier mass loss in the early twenty-first century, *Nature*, 592, 726–731, <https://doi.org/10.1038/s41586-021-03436-z>, 2021.
- Hulth, J., Denby, C. R., and Hock, R.: Estimating glacier snow accumulation from backward calculation of melt and snowline tracking, *Annals of glaciology*, 54, 1–7, <https://doi.org/10.3189/2013AoG62A083>, 2013.
- 500 Huss, M.: Density assumptions for converting geodetic glacier volume change to mass change, *The Cryosphere*, 7, 877–887, <https://doi.org/10.5194/tc-7-877-2013>, 2013.
- Huss, M. and Hock, R.: Global-scale hydrological response to future glacier mass loss, *Nature Climate Change*, 8, 135–140, <https://doi.org/10.1038/s41558-017-0049-x>, 2018.
- 505 Huss, M., Bauder, A., Funk, M., and Hock, R.: Determination of the seasonal mass balance of four Alpine glaciers since 1865, *Journal of Geophysical Research: Earth Surface*, 113, <https://doi.org/10.1029/2007JF000803>, 2008.
- Huss, M., Hock, R., Bauder, A., and Funk, M.: Conventional versus reference-surface mass balance, *Journal of Glaciology*, 58, 278–286, <https://doi.org/10.3189/2012JoG11J216>, 2012.
- Huss, M., Sold, L., Hoelzle, M., Stokvis, M., Salzmann, N., Farinotti, D., and Zemp, M.: Towards remote monitoring of sub-seasonal glacier mass balance, *Annals of Glaciology*, 54, 75–83, <https://doi.org/10.3189/2013AoG63A427>, 2013.
- 510 Huss, M., Dhulst, L., and Bauder, A.: New long-term mass-balance series for the Swiss Alps, *Journal of Glaciology*, 61, 551–562, <https://doi.org/10.3189/2015JoG15J015>, 2015.
- Immerzeel, W. W., Lutz, A., Andrade, M., Bahl, A., Biemans, H., Bolch, T., Hyde, S., Brumby, S., Davies, B., Elmore, A., et al.: Importance and vulnerability of the world’s water towers, *Nature*, 577, 364–369, <https://doi.org/10.1038/s41586-019-1822-y>, 2020.
- 515 Klug, C., Bollmann, E., Galos, S. P., Nicholson, L., Prinz, R., Rieg, L., Sailer, R., Stötter, J., and Kaser, G.: Geodetic reanalysis of annual glaciological mass balances (2001–2011) of Hintereisferner, Austria, *The Cryosphere*, 12, 833–849, <https://doi.org/10.5194/tc-12-833-2018>, 2018.
- Kuhn, M., Markl, G., Kaser, G., Nickus, U., Obleitner, F., and Schneider, H.: Fluctuations of climate and mass balance: different responses of two adjacent glaciers, *Zeitschrift für Gletscherkunde und Glazialgeologie*, 21, 409–416, 1985.
- 520 Landmann, J. M., Künsch, H. R., Huss, M., Ogier, C., Kalisch, M., and Farinotti, D.: Assimilating near-real-time mass balance stake readings into a model ensemble using a particle filter, *The Cryosphere*, 15, 5017–5040, <https://doi.org/10.5194/tc-15-5017-2021>, 2021.
- Linsbauer, A., Huss, M., Hodel, E., Bauder, A., Fischer, M., Weidmann, Y., Bärtschi, H., and Schmassmann, E.: The New Swiss Glacier Inventory SGI2016: from a topographical to a glaciological dataset, *Frontiers in Earth Science*, 9, 774, <https://doi.org/10.3389/feart.2021.704189>, 2021.
- 525 Mannerfelt, E. S., Dehecq, A., Hugonnet, R., Hodel, E., Huss, M., Bauder, A., and Farinotti, D.: Halving of Swiss glacier volume since 1931 observed from terrestrial image photogrammetry, *The Cryosphere*, 16, 3249–3268, <https://doi.org/10.5194/tc-16-3249-2022>, 2022.



- MeteoSwiss: Daily, monthly and yearly satellite-based global radiation, Tech. rep., Available at: https://www.meteoswiss.admin.ch/content/dam/meteoswiss/en/climate/swiss-climate-in-detail/doc/ProdDoc_SIS.pdf, last accessed: 28 October 2021, 2018.
- 530 MeteoSwiss: Documentation of MeteoSwiss Grid-Data Products: Daily Mean, Minimum and Maximum Temperature: TabsD, TminD, TmaxD, Available at: https://www.meteoswiss.admin.ch/content/dam/meteoswiss/de/service-und-publikationen/produkt/raeumliche-daten-temperatur/doc/ProdDoc_TabsD.pdf, last accessed: September 2021, 2021a.
- MeteoSwiss: Daily Precipitation (final analysis): RhiresD, Tech. rep., Available at: https://www.meteoswiss.admin.ch/content/dam/meteoswiss/de/service-und-publikationen/produkt/raeumliche-daten-niederschlag/doc/ProdDoc_RhiresD.pdf, last accessed: 28 October 2021, 2021b.
- 535 Möller, M. and Schneider, C.: Calibration of glacier volume–area relations from surface extent fluctuations and application to future glacier change, *Journal of Glaciology*, 56, 33–40, <https://doi.org/10.3189/002214310791190866>, 2010.
- Nicholson, L. and Benn, D. I.: Properties of natural supraglacial debris in relation to modelling sub-debris ice ablation, *Earth Surface Processes and Landforms*, 38, 490–501, <https://doi.org/10.1002/esp.3299>, 2012.
- Patro, E. R., De Michele, C., and Avanzi, F.: Future perspectives of run-of-the-river hydropower and the impact of glaciers’ shrinkage: The case of Italian Alps, *Applied Energy*, 231, 699–713, <https://doi.org/10.1016/j.apenergy.2018.09.063>, 2018.
- 540 Pellicciotti, F., Brock, B., Strasser, U., Burlando, P., Funk, M., and Corripio, J.: An enhanced temperature-index glacier melt model including the shortwave radiation balance: development and testing for Haut Glacier d’Arolla, Switzerland, *Journal of Glaciology*, 51, 573–587, <https://doi.org/10.3189/172756505781829124>, 2005.
- Pellicciotti, F., Carenzo, M., Bordoy, R., and Stoffel, M.: Changes in glaciers in the Swiss Alps and impact on basin hydrology: current state of the art and future research, *Science of the Total Environment*, 493, 1152–1170, 2014.
- 545 Pfeifer, N., Mandlbürger, G., Otepka, J., and Karel, W.: OPALS—A framework for Airborne Laser Scanning data analysis, *Computers, Environment and Urban Systems*, 45, 125–136, <https://doi.org/10.1016/j.compenvurbsys.2013.11.002>, 2014.
- Piermattei, L., Zemp, M., Sommer, C., Brun, F., Braun, M. H., Andreassen, L. M., Belart, J. M., Berthier, E., Bhattacharya, A., Boehm Vock, L., et al.: Observing glacier elevation changes from spaceborne optical and radar sensors—an inter-comparison experiment using ASTER and TanDEM-X data, *The Cryosphere*, 18, 3195–3230, <https://doi.org/10.5194/tc-18-3195-2024>, 2024.
- 550 Radić, V. and Hock, R.: Glaciers in the Earth’s hydrological cycle: assessments of glacier mass and runoff changes on global and regional scales, *Surveys in Geophysics*, 35, 813–837, 2014.
- Rounce, D. R., Hock, R., and Shean, D. E.: Glacier mass change in High Mountain Asia through 2100 using the open-source python glacier evolution model (PyGEM), *Frontiers in Earth Science*, 7, 331, <https://doi.org/10.3389/feart.2019.00331>, 2020.
- 555 Rounce, D. R., Hock, R., McNabb, R., Millan, R., Sommer, C., Braun, M., Malz, P., Maussion, F., Mouginot, J., Seehaus, T., et al.: Distributed global debris thickness estimates reveal debris significantly impacts glacier mass balance, *Geophysical Research Letters*, 48, e2020GL091311, <https://doi.org/10.1029/2020GL091311>, 2021.
- Rounce, D. R., Hock, R., Maussion, F., Hugonnet, R., Kochtitzky, W., Huss, M., Berthier, E., Brinkerhoff, D., Compagno, L., Copland, L., Farinotti, D., Menounos, B., and McNabb, R. R.: Global glacier change in the 21st century: Every increase in temperature matters, *Science*, 379, 78–83, <https://doi.org/10.1126/science.abo1324>, 2023.
- 560 Salzmann, N., Machguth, H., and Linsbauer, A.: The Swiss Alpine glaciers’ response to the global ‘2° C air temperature target’, *Environmental Research Letters*, 7, 044001, <https://doi.org/10.1088/1748-9326/7/4/044001>, 2012.
- Schaeffli, B., Manso, P., Fischer, M., Huss, M., and Farinotti, D.: The role of glacier retreat for Swiss hydropower production, *Renewable Energy*, 132, 615–627, <https://doi.org/10.1016/j.renene.2018.07.104>, 2019.



- 565 Schuster, L., Rounce, D. R., and Maussion, F.: Glacier projections sensitivity to temperature-index model choices and calibration strategies, *Annals of Glaciology*, pp. 1–16, <https://doi.org/10.1017/aog.2023.57>, 2023.
- Schwaizer, G., Nemec, J., Nagler, T., Mölg, N., and Paul, F.: Automated Classification of Glacier Facies From Sentinel-2 And Landsat Data, in: *Remote Sensing of the Cryosphere: Methods and Applications from Regional to Global Scale*, 10th EARSeL Workshop, pp. 145–146, Bern, CH, 2023.
- 570 Stoffel, M. and Huggel, C.: Effects of climate change on mass movements in mountain environments, *Progress in Physical Geography*, 36, 421–439, <https://doi.org/10.1177/0309133312441010>, 2012.
- swisstopo: swisstopo swissALTI3D, Available at: <https://www.swisstopo.admin.ch/en/height-model-swissalti3d>, last accessed: 8 June 2020, 2020.
- swisstopo: swissALTI3D Das hoch aufgelöste Terrainmodell der Schweiz: Detaillierte Produktinfo, Tech. rep., Swiss Federal Office of Topography, 2022.
- 575 swisstopo: Spezialbefliegungen. Data set, provided to the Laboratory of Hydraulics, Hydrology and Glaciology (VAW), ETH Zürich by swisstopo, 2024.
- The GLAMBIE Team: Community estimate of global glacier mass changes from 2000 to 2023, *Nature*, 639, 382–388, <https://doi.org/10.1038/s41586-024-08545-z>, 2025.
- 580 van der Meer, M., Zekollari, H., Huss, M., Bolibar, J., Sjurssen, K. H., and Farinotti, D.: A minimal machine-learning glacier mass balance model, *The Cryosphere*, 19, 805–826, <https://doi.org/10.5194/tc-19-805-2025>, 2025.
- van Tiel, M., Huss, M., Zappa, M., Jonas, T., and Farinotti, D.: Swiss glacier mass loss during the 2022 drought: persistent streamflow contributions amid declining melt water volumes, *EGUsphere*, 2025, 1–29, <https://doi.org/10.5194/egusphere-2025-404>, 2025.
- Vincent, C., Cusicanqui, D., Jourdain, B., Laarman, O., Six, D., Gilbert, A., Walpersdorf, A., Rabatel, A., Piard, L., Gimbert, F., et al.: Geodetic point surface mass balances: a new approach to determine point surface mass balances on glaciers from remote sensing measurements, *The Cryosphere*, 15, 1259–1276, <https://doi.org/10.5194/tc-15-1259-2021>, 2021.
- 585 Voordendag, A., Prinz, R., Schuster, L., and Kaser, G.: Brief communication: The Glacier Loss Day as an indicator of a record-breaking negative glacier mass balance in 2022, *The Cryosphere*, 17, 3661–3665, <https://doi.org/10.5194/tc-17-3661-2023>, 2023.
- xdem contributors: xdem, <https://doi.org/10.5281/zenodo.4809698>, 2021.
- 590 Zekollari, H., Huss, M., and Farinotti, D.: Modelling the future evolution of glaciers in the European Alps under the EURO-CORDEX RCM ensemble, *The Cryosphere*, 13, 1125–1146, <https://doi.org/10.5194/tc-13-1125-2019>, 2019.
- Zeller, L., McGrath, D., Sass, L., O’Neel, S., McNeil, C., and Baker, E.: Beyond glacier-wide mass balances: parsing seasonal elevation change into spatially resolved patterns of accumulation and ablation at Wolverine Glacier, Alaska, *Journal of Glaciology*, 69, 87–102, <https://doi.org/10.1017/jog.2022.46>, 2022.
- 595 Zemp, M., Huss, M., Thibert, E., Eckert, N., McNabb, R., Huber, J., Barandun, M., Machguth, H., Nussbaumer, S. U., Gärtner-Roer, I., et al.: Global glacier mass changes and their contributions to sea-level rise from 1961 to 2016, *Nature*, 568, 382–386, <https://doi.org/10.1038/s41586-019-1071-0>, 2019.
- Zhang, W., Gu, X., Tang, L., Yin, Y., Liu, D., and Zhang, Y.: Application of machine learning, deep learning and optimization algorithms in geoenvironment and geoscience: comprehensive review and future challenge, *Gondwana Research*, 109, 1–17, <https://doi.org/10.1016/j.gr.2022.03.015>, 2022.
- 600